Spectroscopic Studies of the Dark Space ahead of a Shock Wave in an Argon Plasma Flow

Michio Nishida and Akihiko Nakajima
Department of Aeronautical Engineering, Kyoto University, Kyoto, Japan

Z. Naturforsch. **38 a**, 802–807 (1983); received September 1, 1982

Spectroscopic studies of the dark space ahead of a detached shock wave caused by a blunt body were made in a partially ionized argon flow. From emission measurements, spatially resolved population densities of states 5p [3/2], 5p [5/2] and 4p [3/2] were determined at 20 stations in the flow, for both cases when the blunt body is placed in the flow and when it is withdrawn. The result shows that the population densities of the above mentioned states ahead of the shock wave are reduced when the body is placed in the flow. A prediction was obtained by assuming a steady state population for all levels higher than level 4s. In the prediction the measured electron temperatures and densities were employed to determine collisional transition probabilities. From a comparison of the experiment with the prediction, it is considered that the dark space is caused by the elevation in the electron temperature ahead of the shock wave.

I. Introduction

When a blunt body is placed in a flow of ionized gas, a region of reduced self-luminosity can be observed ahead of the detached shock wave of the body. This region is called the "dark space". According to Grewal and Talbot [1] there exists a broad zone of elevated electron temperature ahead of the electron compression region, caused by the high thermal conductivity of the electron gas. The electron density being unchanged in this zone, the elevated electron temperature reduces the recombination rate and thus the self-luminosity of the flow.

The self-luminosity is caused by radiative transitions between levels of bound electrons. For argon, the strongest visible spectral lines result from the transitions 5 p → 4 s and 4 p → 4 s, so that the reduction in the number of atoms excited in the electronic levels 5 p and 4 p is expected to make the dark space.

Since the study by Grewal and Talbot [1]. Christiansen [2] has measured the radiation intensity upstream of the shock wave and Kirchhof and Talbot [3] have calculated the recombination rate in the dark space using the collisional-radiative model of recombination given by Hinnov and Hirschberg [4] in combination with measured electron temperature and density data. They found that the minimum in the recombination rate occurs at the point of minimum luminosity in the dark space. In a study by one of the authors [5], the population density distributions of 20 electronic levels from the free stream to the blunt body wall were obtained by solving the rate equations for excited atoms coupled with the electron energy equation.

The present work is concerned with measurements of the axial variation of excited level population densities upstream of the shock wave, caused by a blunt body, and a comparison of these with theoretical predictions. The spatially resolved population densities were obtained by making absolute radiation intensity measurements and by using the Abel inversion. Predictions were obtained by solving the rate equations for electronic level occupations, wherein observed electron temperatures and densities were employed to determine collisional transition probabilities.

II. Experimental Procedure

The experiments were carried out in a low density plasma wind tunnel operated by a dc arc type discharge. A schematic diagram of the set up is shown in Figure 1. Argon, after being heated and partially ionized by an arc heater, flows into a plenum chamber and then expands through a convergent-divergent nozzle into a test section. The throat and exit diameters of the nozzle are 1.36 cm and 5 cm, respectively, and the half-cone angle is 15°. A blunt body having a nose radius of 4 cm was

Reprint requests to Prof. M. Nishida, Department of Aeronautical Engineering, Kyoto University, Kyoto/Japan.

0340-4811 / 83 / 0700-0802 $ 01.3 0/0. – Please order a reprint rather than making your own copy.

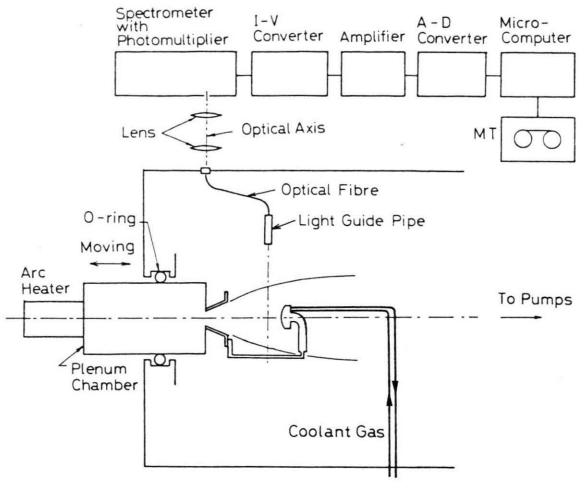

Fig. 1. Schematic diagram of experiment.

placed at a location 8.5 cm from the nozzle exit. The body was electrically insulated from the tunnel wall, so that the potential on the body was the floating potential. The surface temperature of the body was controlled by cooling the body with nitrogen gas, which was kept within 402 and 412 K. Since the blunt body is connected to the nozzle, as shown in Fig. 1, spectroscopic measurements were possible at any axial station between the nozzle exit and the body wall, by varying the position of the nozzle relative to the optical axis.

Typical operating conditions were as follows: argon mass flow rate = 0.11 g/s, stagnation pressure = 1.8 kPa, test section pressure = 10 Pa, stagnation temperature = 3400 K. Flow parameters along the centerline were estimated from impact-pressure measurements and the stagnation conditions by using the isentropic flow relationship. The stagnation temperature was calculated by using the simple choked flow relationship as given in [6]. Under our flow conditions, the Mach number was 4.0 at the nozzle exit and 4.4 at the blunt body position. Consequently, the atom density was estimated to be 1.9×10^{21} particles/m^3 at the body position. From a comparison of the atom density with the observed electron density, the degree of ionization is seen to be much smaller than unity, so that the overall flow field is expected to be governed by neutral atoms. Under the assumption of a viscous shock layer, shock layer equations were numerically solved to estimate the shock layer thickness. This was found to be 0.67 cm. In this calculation, a partially ionized gas assumption was employed.

The optical system is also depicted in Figure 1. A lens mounted in a light guide pipe with 2.5 mm × 2.5 mm cross section collects light coming from the plasma and focuses it onto the end of an optical fibre. The light emitted from the other end of this optical fibre is refocused by two lenses onto the entrance slit of a spectrometer which is equipped with a photomultiplier tube. The output from this photomultiplier tube is sent to an AD converter which samples digital data every 25 ms. The data are recorded on a magnetic cassette tape which is controlled by a micro-computer. These are then read and processed by a large computer. The optical system was calibrated for absolute intensity measurements by using a standard tungsten ribbon filament lamp. After the Abel inversion for radial data was made on the computer, the spatially resolved population densities were determined.

The emission measurements were made on the lines at 4300 Å, 4159 Å and 7635 Å. These measurements were carried out at 20 stations between 7 cm and 0.2 cm upstream of the blunt body. The population densities of states 5p [5/2], 5p [3/2] and 4p [3/2] were then deduced from the data of 4300 Å, 4159 Å and 7635 Å, respectively.

Electrostatic-probe measurements were also made to determine the electron temperature and density. The measured values of these were employed for estimating the collisional transition probabilities which were used in the prediction of the population densities.

III. Theoretical Prediction

The excited level model employed in this work is the same as that used in the earlier work [5]. The present model contains 20 excited levels, and the populations of the highly excited levels above 9s can be assumed to be in equilibrium with free electrons. Under the present conditions, the characteristic flow time of the gas is of the order of 10^{-5} s, while the relaxation time of the excited levels above level 4s is of an order less than 10^{-8} s. A steady state assumption may, therefore, be made for the levels from level 4p ($j = 3$) to level 9s ($j = 20$), which leads to the equation

$$\dot{n}(j) = 0, \quad j = 3, 4, \ldots, 20, \tag{1}$$

where $\dot{n}(j)$ is the net production rate of the population density of level j. On the other hand, the relaxa-

tion time of level 4s is in the range from 10^{-6} s to 10^{-4} s, under an assumption that, to a first approximation, the radiation originating from level 4s is trapped. This means that the steady state assumption does not hold for this level but we have

$$\mathrm{d}[n(2)/n]/\mathrm{d}y = \dot{n}(2)/nu\,, \tag{2}$$

where $n(2)$ is the population density of level 4s ($j=2$), n the global density, and u the flow velocity. y is taken in the direction of the flow. $\dot{n}(j)$ is expressed as

$$\begin{aligned}\dot{n}(j) = &\sum_{s=1}^{\infty}[Q(s,j)\,n_e n(s) - Q(j,s)\,n_e n(j)] \\ &+ Q_R(\infty,j)\,n_e^2 - Q_I(j,\infty)\,n_e n(j) \\ &+ \sum_{s=j+1}^{\infty}\beta(s,j)\,A(s,j)\,n(s) \\ &- \sum_{s=1}^{j-1}\beta(j,s)\,A(j,s)\,n(j) \\ &+ \beta(\infty,j)\,A(\infty,j)\,n_e^2\,,\end{aligned} \tag{3}$$

where n_e is the electron density, $Q(s,j)$ the rate constant for an electron-collisional transition from level s to level j, $Q_I(j,\infty)$ is the collisional ionization rate constant from level j, $Q_R(\infty,j)$ the collisional recombination rate constant to level j, $A(s,j)$ is the radiative transition rate constant from level s to level j, $A(\infty,j)$ the radiative recombination rate constant to level j, and $\beta(j,s)$ is the radiative escape factor.

For the present work, Drawin's [7] expression for the excitation rate constants was employed, which, for optically allowed transitions gives

$$\begin{aligned}Q(j,k) = &\,4\pi a_0^2 \bar{v}\,(Ry/k_B T_e)^2 \\ &\cdot f(j,k)\,K(j,k)/\{u(j,k)[u(j,k)+1]\} \\ &\cdot \exp[-u(j,k)]\left\{\frac{1}{20+u(j,k)}\right. \\ &\left.+\ln\left[1.25\,\delta(j,k)\left(1+\frac{1}{u(j,k)}\right)\right]\right\}\,,\end{aligned} \tag{4}$$

and, for parity forbidden transitions

$$\begin{aligned}Q(j,k) = &\,4\pi a_0^2 \bar{v}\,K(j,k)\,u(j,k)\left\{\frac{\exp[-u(j,k)]}{u(j,k)}\right. \\ &\left.-\int_{u(j,k)}^{\infty}\frac{\exp(-x)}{x}\,\mathrm{d}x\right\}.\end{aligned} \tag{5}$$

Here a_0 is the first Bohr radius, Ry the Rydberg constant, $\bar{v}$ the mean electron velocity expressed as $(8k_B T_e/\pi m_e)^{1/2}$, k_B the Boltzmann constant, T_e is the electron temperature, $f(j,k)$ the absorption oscillator strength, $K(j,k)$ the parameter introduced to achieve numerical agreement with experiment, $\delta(j,k)$ the shape parameter, and

$$u(j,k) = |E(j) - E(k)|/k_B T_e\,,$$

in which $E(j)$ is the excitation energy. The ionization rate constant, $Q_I(j,\infty)$, can be easily obtained by replacing $u(j,k)$ with $u(j,\infty)$ in (4), and taking $f(j,k)$, $K(j,k)$ and $\delta(j,k)$ as unity. Using the principle of detailed balancing, the recombination rate constant, $Q_R(\infty,j)$, is also easily determined.

The shape parameter $\delta(j,k)$ is assumed to be unity for all transitions except for the $3p-4s$ transition which is taken to be 0.8 [8]. The parameter $K(j,k)$ was estimated from matching Drawin's cross section for electronic excitation to the cross section determined by using the multipole expansion method proposed by Sobelman [9].

According to Drawin and Emard [10], the collisional frequencies for atom-collisional transitions are negligible compared with those for electron-collisional transitions under the present conditions, so that the atom-collisional transitions are ignored. The radiative transition rate constants were calculated from the direct integration of the wave function given by Bates and Damgaard [11]. To a first approximation, radiations terminated in any level except for the ground level are taken to be optically thin, which leads to the radiative escape factor being unity. On the other hand, absorption coefficients for radiations terminated in the ground level are large enough to assume almost immediate capture of all emissions. It is therefore appropriate to take the radiative escape factor to be zero for these conditions.

Equations (1) and (2) coupled with (3) to (5) can be solved to provide the population densities of all the levels. In the calculations, the electron temperature and density, flow velocity, and global density are needed. The electron temperature and density are obtained from the experimental data. The flow velocity and global density are deduced from the stagnation conditions and impact-pressure measurements.

IV. Results

Figure 2 shows the distributions of the electron temperature and density measured on the flow

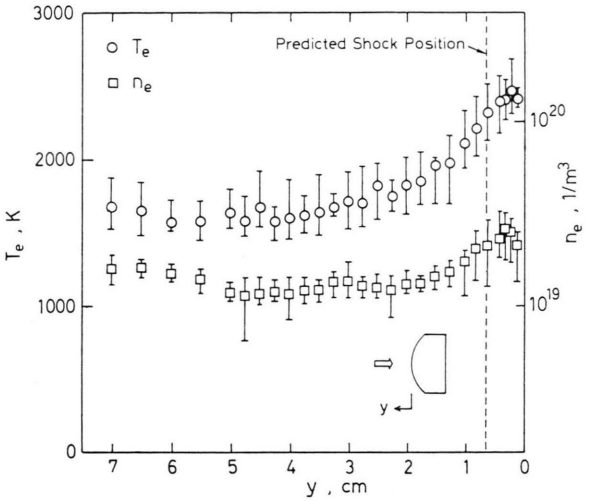

Fig. 2. Distribution of electron temperature and density.

centerline. The electron temperature rises in the region from $y = 3.75$ cm to $y = 0.2$ cm, where it reaches 2500 K (y is taken as the distance from the body wall). It should be noted that the electron density is nearly constant in the region from $y = 3.75$ cm to $y = 2.75$ cm, while the electron temperature rises in this region.

In Fig. 3 two population density distributions on the flow centerline with and without the presence of the blunt body are shown. In a case of the presence of the blunt body the population densities evidently fall below those in its absence, in a zone from $y = 3.5$ cm to $y = 1.25$ cm. This is the dark space. The population densities of both states rapidly increase in the region from $y = 1.5$ cm to $y = 0.4$ cm. This is due to the shock wave. The ratio of the maximum population density at $y = 0.4$ cm to the minimum at $y = 1.5$ cm is 4.2 for state 5 p [3/2], and 4.8 for state 5 p [5/2].

These ratios are higher than the ratio from the Rankine-Hugoniot relationship, namely 3.5, because the ratio of the population densities of electronic levels ahead of and behind the shock wave cannot be determined from the Rankine-Hugoniot relationship but has to be derived from steady state populations.

Figure 4 shows corresponding population density distributions of the state 4p [3/2]. The two results for the presence of the body relate to the absorption of ArI7635 radiation by atoms in state 4s [3/2]° being or being not taken into account in the Abel inversion. The radial profiles of the absolute density of absorbers (atoms in state 4s [3/2]°) and their temperature are required for the absorption to be taken into account in the Abel inversion. The population densities of state 4s [3/2]° on the flow centerline were determined by assuming an isentropic flow because we had no experimental data for the axial distribution of the 4s-level atom density. Also, the radial profile at each station was approximated by that obtained by Limbaugh [12]. It

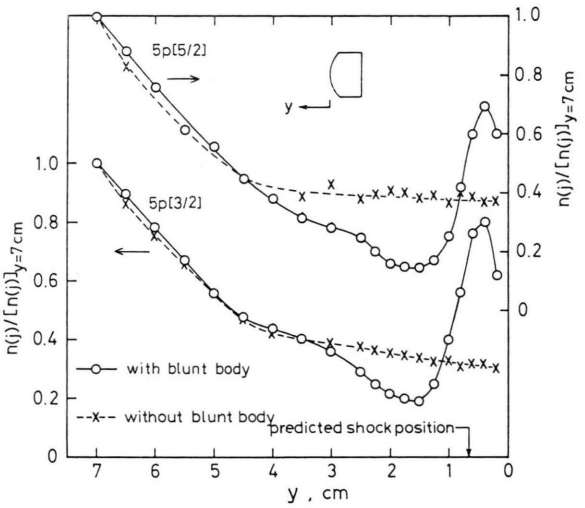

Fig. 3. Population density distribution of states 5p [3/2] and 5p [5/2] with and without a blunt body.

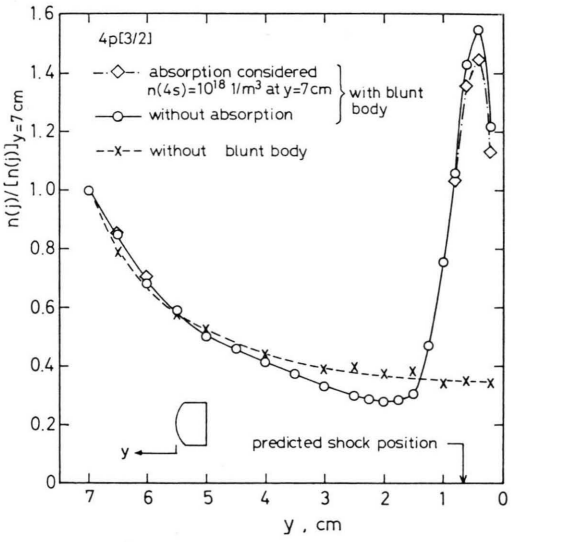

Fig. 4. Population density distribution of state 4p [3/2] with and without a blunt body.

was assumed that the jet radii of the emitter (atoms in state 4p [3/2]) and absorber (atoms in state 4s [3/2]°) are approximately equal. It was also assumed that the absorber temperature is constant in the radial direction. In addition, Doppler broadening was taken for the spectral line. An population density distribution obtained by this method is shwon in Fig. 4, normalized by the population density at $y = 7$ cm. In considering absorption, the population density of state 4s [3/2]° at $y = 7$ cm was taken to be 10^{18} particles/m^3, and then 10^{16} particles/m^3. The result for the latter case is nearly the same as that obtained without absorption. Even when the population density of 4s [3/2]° at $y = 7$ cm is taken to be 10^{18} particles/m^3, the population density is only slightly smaller than that for the case without absorption. In Fig. 4 the population density obtained when the body is placed in the flow falls below that without the body, in the zone from $y = 4$ cm to $y = 1.5$ cm. This zone is also the dark space for the ArI7635 radiation. The ratio of the maximum population density at $y = 0.4$ cm to the minimum at $y = 2$ cm is 4.13. This value is noticeably higher than that predicted from the Rankine-Hugoniot relationship.

V. Comparison of Experiment with Theory

It is of interest to compare the observed population density distributions with the predicted ones based on the measured electron temperatures and densities. The comparisons for states 5p [3/2] and 5p [5/2] are shown in Fig. 5 and that for state 4p [3/2] is shown in Figure 6. In these figures $g(j)$ is the statistical weight of state j.

We tried to solve (2) for three different boundary conditions of $n(2)/g(2)$ at $y = 7$ cm, i.e. 10^{15}, 10^{16} and 10^{17} particles/m^3, where $g(2)$ is the statistical weight of level 4s ($j = 2$). The reason for the choice of these values is that the 4s-level population densities observed in Ref. [13] fall in this region. The predicted results for the three boundary conditions were very close. This is because, under the present conditions, de-excitations to level 4s are very dominant compared to the inverse transitions.

In Fig. 5, the predicted distributions are similar to the experimental ones upstream of the shock wave, though the prediction indicates a somewhat slower decrease than the experiment. In the whole region the predicted population density decreases

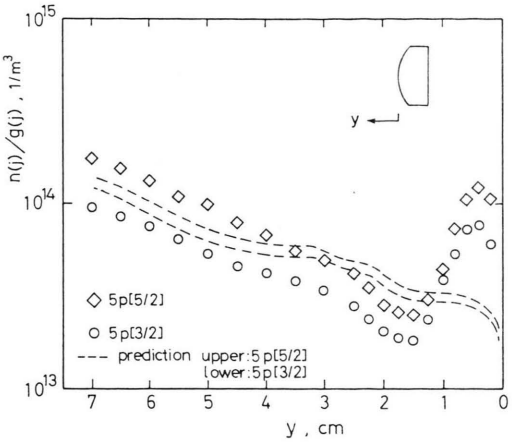

Fig. 5. Comparison of experiment with prediction for states 5p [3/2] and 5p [5/2].

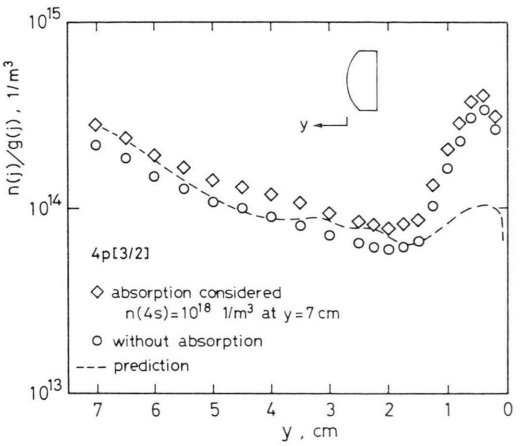

Fig. 6. Comparison of experiment with prediction for state 4p [3/2].

toward the wall. The decrease in the region, $y = 7$ cm to $y = 4.5$ cm, is due to the decrease in the electron density. The predicted population density continues decreasing from $y = 4.5$ cm to $y = 1.75$ cm in spite of almost constant electron density. On the other hand, the electron temperature in this region is elevated. In the region $y = 1.25$ cm to $y = 0.75$ cm, the predicted population density is nearly constant and then rapidly decreases. This prediction significantly deviates from the experimental results perhaps because it is based on the simple one-dimensional analysis that is only valid in the free-stream region ahead of the shock wave. It is questionable to extend this analysis to the shock-layer region. In the shock layer, two-dimensional

treatment will be required. Furthermore, diffusion must be included into this analysis. According to Drawin and Emard [14, 15], diffusion plays an important role to determine population densities. Adding a diffusion term to the rate equations will lead to higher population densities. This is our future problem.

The result for state 4p [3/2] is shown in Fig. 6. The experimental population density decreases in the region $y = 7$ cm to $y = 2$ cm, and then increases. The predicted distribution is very similar to the experimental one, but in the downstream of $y = 1.5$ cm the predicted population density increases less rapidly than the experimental one. The decrease in the predicted density in the region $y = 7$ cm to $y = 4.5$ cm is due to the decrease in the electron density. The prediction shows the reduced population density in the region $y = 4.5$ cm to $y = 2$ cm, despite of nearly constant electron density. In this region, the electron temperature is elevated.

VI. Concluding Remarks

Spectroscopic measurements of plasma flows were made with and without a blunt body placed in the flow. In the former case the population densities of states 5p [3/2], 5p [5/2] and 4p [3/2] observed ahead of the detached shock wave are lower than in the latter case. In the region of the lower population density, the electron density is nearly constant while the electron temperature is higher. The population density distribution predicted by using the observed electron temperatures and densities shows the lower population density in the region where the electron temperature is elevated. The comparison of the experiment with the prediction shows that the reduction in the population densities of states 5p [3/2], 5p [5/2] and 4p [3/2] is caused by the elevation in the electron temperature ahead of the shock wave. This elevation results from the high thermal conduction of the electrons and the high temperature region behind the shock wave. As the electron temperature increases, the equilibrium population densities of upper levels will be reduced. This transition to lower levels occurs through collisional and radiative de-excitation. Thus the population densities of levels 4p and 5p are reduced, which leads to the dark space. Therefore, the dark space can be observed in the plasma only where highly lying level populations are in equilibrium with free electrons and where the transitions between highly lying levels are controlled by electron collisions.

[1] M. S. Grewal and L. Talbot, J. Fluid Mech. **16,** 573 (1963).
[2] W. H. Christiansen, Phys. Fluids **10,** 2586 (1967).
[3] R. H. Kirchhof and L. Talbot, AIAA J. **9,** 1098 (1971).
[4] E. Hinnov and J. G. Hirschberg, Phys. Rev. **125,** 795 (1962).
[5] M. Nishida, Z. Naturforsch. **36a,** 980 (1981).
[6] R. B. Fraser, F. Robben, and L. Talbot, Phys. Fluids **14,** 2317 (1971).
[7] H. W. Drawin, EUR-CEA-FC-383, Association Euratom-C.E.A., Fontenay-aux-Roses, France, 1967.
[8] K. Katsonis, EUR-CEA-FC-820, Association Euratom-C.E.A., Fontenay-aux-Roses, France, 1976.
[9] I. I. Sobelman, Introduction to the Theory of Atomic Spectra, Pergamon Press, Oxford 1972, Capter 11.
[10] H. W. Drawin and F. Emard, Phys. Letters **43A,** 333 (1973).
[11] D. R. Bates and A. Damgaard, Phil. Trans. Roy. Soc. London **A242,** 101 (1949).
[12] C. C. Limbaugh, Rarefield Gas Dynamics, edited by J. L. Potter, AIAA Progress Series, **51,** 933 (1977).
[13] A. Kimura, K. Tanaka, and M. Nishida, Rarefied Gas Dynamics, edited by S. S. Fisher, AIAA Progress Series, Vol. **74,** 1155 (1981).
[14] H. W. Drawin and F. Emard, Z. Naturforsch. **28a,** 1289 and 1422 (1973).
[15] H. W. Drawin and F. Emard, Z. Phys. **186,** 99 (1965).